IEEE Photonics Journal
An IEEE Photonics Society Publication

Polarization-Independent Surface Plasmon Liquid Crystal Photonic Crystal Multiplexer–Demultiplexer

Volume 7, Number 5, October 2015

Mohamed Farhat O. Hameed, Member, IEEE
R. T. Balat
A. M. Heikal
Mervat M. Abo-Elkhier
M. I. Abo el Maaty
S. S. A. Obayya, Senior Member, IEEE

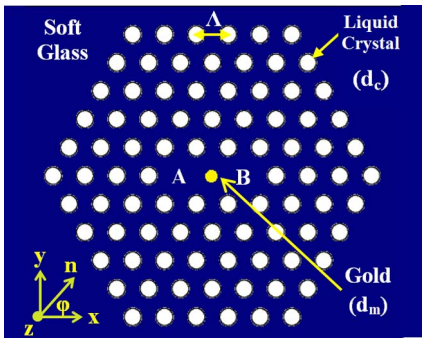

DOI: 10.1109/JPHOT.2015.2480538
1943-0655 © 2015 IEEE

Polarization-Independent Surface Plasmon Liquid Crystal Photonic Crystal Multiplexer–Demultiplexer

Mohamed Farhat O. Hameed,[1,2] *Member, IEEE*, R. T. Balat,[2] A. M. Heikal,[1,3] Mervat M. Abo-Elkhier,[2] M. I. Abo el Maaty,[2] and S. S. A. Obayya,[1] *Senior Member, IEEE*

[1]Center for Photonics and Smart Materials, Zewail City of Science and Technology, Giza 12588, Egypt
[2]Department of Mathematics and Engineering Physics, Faculty of Engineering, Mansoura University, Mansoura 35516, Egypt
[3]Department of Electronics and Communications Engineering, Faculty of Engineering, Mansoura University, Mansoura 35516, Egypt

DOI: 10.1109/JPHOT.2015.2480538

Manuscript received August 16, 2015; revised September 12, 2015; accepted September 15, 2015. Date of publication September 22, 2015; date of current version September 30, 2015. Corresponding author: S. S. A. Obayya (e-mail: sobayya@zewailcity.edu.eg).

Abstract: A novel design of polarization-independent surface plasmon multiplexer–demultiplexer (MUX/DEMUX) based on dual-core photonic crystal fiber with a central gold wire is proposed and analyzed. The cladding air holes are infiltrated with a nematic liquid crystal of type E7 with rotation angle φ, and the background material is a soft glass of type SF57 (lead silica). The simulation results are obtained using full-vectorial finite-difference method and coupled mode theory. At $\varphi = 90°$, the suggested MUX/DEMUX has a short device length of 953.254 μm for x-polarized modes with broad bandwidths of 235 and 175 nm around wavelengths of 1.3 and 1.55 μm, respectively, with low cross-talk better than –20 dB. For y-polarized modes, the reported MUX/DEMUX has short device length of 1322.86 μm with broad bandwidths of 193 and 170 nm around 1.3 and 1.55 μm, respectively. Moreover, the polarization independence is achieved with short device lengths of 1138.06 and 1180 μm at $\varphi = 90°$ and 0°, respectively.

Index Terms: Polarization-independent device, multiplexer–demultiplexer, plasmonics, couple mode theory, liquid crystal, finite-difference method.

1. Introduction

Photonic crystal fibers (PCFs) [1], [2] have become one of the most important topics for recent investigations. PCF can be endlessly single mode and can be tailored to achieve nearly zero and flat dispersion over a wide wavelength range. Such unique characteristics of PCFs have sparked growing interest in their use in many fields, from theory to applications. PCFs are usually formed by a defect region surrounded by microstructured air hole cladding. The mode field can be confined in solid core defect by modified total internal reflection between high refractive index core and low refractive index cladding region. Additionally, the light can be confined in a low index core by the photonic bandgap guidance. The polarization effect through PCFs can be investigated by filling the cladding air holes with liquid crystal (LC) [3], [4] or metal [5].

PCFs filled with metallic nanowires have been successfully fabricated by blocking selected holes of PCF and filling them with liquid gold [6]. Additionally, direct drawing fiber from a gold filled fused-silica cane [7] can be used for filling PCFs with metallic nanowires. Surface waves supported by metal-dielectric interface, known as surface plasmons (SPs) which are transformed to surface plasmon polaritons (SPPs) when they are coupled to externally applied electromagnetic waves, have attracted a lot of interest in recent years [8]. The PCF, as the dielectric medium, guides the core modes and the metal wire guides the SPP modes. In the metal-filled PCF, at certain resonant wavelength, the guided core modes and the SPP modes can be phase matched. In this case, the surface plasmon resonance (SPR) is achieved, which implies potential applications in fiber based photonic devices. A new approach that uses SPR technology as an optical method has been demonstrated recently in optical sensing [9], [10], optical imaging [11], [12], and polarization beam splitters [13], [14].

The wavelength division multiplexer-demultiplexer (MUX/DEMUX) is of great application value in optical communication systems, since it allows the wavelength multiplexing of 1.3 μm and 1.55 μm bands. This can be used in carrying different data type which increases the transmitted data rate through the optical communication systems. Many studies have been reported in using dual core PCF (DC-PCF) as an optical fiber coupler [15], [16]. In this regard, DC-PCF MUX/DEMUX has been reported [17] with significantly short device length and more design flexibility compared to conventional optical fiber coupler. Due to these advantages, several researchers [15]–[20] have investigated the coupling characteristics of the DC-PCF couplers. In addition, a polarization independent splitter based on highly birefringent DC-PCF is proposed by Florous *et al.* [21]. Moreover, polarization independent splitter based on index guiding all silica based PCF has been introduced by Chen and Zhou [20]. On the other hand, the coupling length of the DC-PCF is strongly dependent on the fiber structure and is still generally long (several millimeters). This can cause problems in many communication applications such as intermodal dispersion in signal pulse transmission [22]. It is therefore no wonder that much effort has recently been devoted to the development of surface-plasmon-based multiplexers [23]. However, polarization-independent MUX-DEMUX based on surface plasmon LC-PCF has not been introduced in the literature. Therefore, this paper is introduced due to the importance of polarization-independent device in many applications.

In this study, for the first time, a novel polarization independent surface plasmon liquid crystal photonic crystal MUX/DEMUX is presented and analyzed. The numerical simulation of the suggested structure is obtained using full vectorial modal solver relying on the finite difference method (FDM) [24] and the coupled mode theory (CMT) [5], [25], [26]. The FDM is a powerful tool which can be used in the modal analysis of different kinds of geometry with high accuracy. Besides, the CMT is applied as a simple mathematical approach that yields an accurate dispersion curves and field patterns for the composite modes and hence the power exchange between the waveguides. The proposed MUX/DEMUX is based on DC LC-PCF with central gold wire and nematic liquid crystal (NLC) of type E7 in the cladding holes. In addition, the background material of the reported MUX-DEMUX is a soft glass of type SF57 (lead silica). The ordinary n_o and extraordinary n_e refractive indices of the E7 material are smaller than that of the SF57 material, which guarantees the index guiding through the core region of the NLC-PCF coupler. Moreover, the infiltration of the NLC increases the birefringence between the two fundamental polarized modes in the proposed design. Further, the SPR can improve the device performance with compact design and easy fabrication process. These features will demonstrate the advantages of the new MUX/DEMUX in complex communication devices. Many studies have been done recently which are mainly focused on the polarization characteristics of fiber waveguides filled with metal [27], [28]. As a new device, the proposed MUX/DEMUX can separate the 1.3 μm and 1.55 μm wavelengths for both x- and y-polarized modes. At $\varphi = 90^\circ$, the suggested MUX/DEMUX is compact in size with shortest coupling length of 953.254 μm for x-polarized modes with broad bandwidth of 235 nm and 175 nm around 1.3 μm and 1.55 μm, respectively, with low crosstalk better than –20 dB. For y-polarized modes, the suggested MUX/DEMUX has short device length of 1322.86 μm with broad bandwidth of 193 nm and 170 nm around 1.3 μm and 1.55 μm,

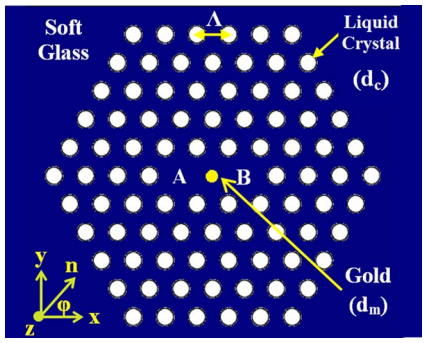

Fig. 1. Cross section of the proposed MUX/DEMUX. The director of the NLC with a rotation angle φ is shown in the inset.

respectively, with low crosstalk better than –20 dB. Moreover, the polarization-independence is achieved with short device length of 1138.06 μm and 1180 μm at $\varphi = 90^\circ$ and 0°, respectively.

Following this introduction, the design considerations and numerical approaches of the proposed MUX/DEMUX is given in Section 2. The numerical results are presented in Section 3. Finally, the conclusion is drawn in Section 4.

2. Design Considerations and Numerical Approaches

Fig. 1 shows cross section of the proposed DC-LCPCF MUX-DEMUX whose cladding holes are infiltrated with NLC of type E7. Additionally, the central hole is filled by gold wire of diameter d_m. Further, the background material is a soft glass of type SF57 (lead silica). The cladding NLC holes of diameter d_C are arranged in hexagonal shape with lattice constant Λ. The NLCs are anisotropic materials, which are characterized by ordinary index n_o, and extraordinary index n_e. The permittivity tensor of the E7 material has the diagonal form $[n_o^2, n_e^2, n_o^2]$, at $\varphi = 90^\circ$ while, the NLC molecules are aligned along x axis at $\varphi = 0^\circ$ with $\varepsilon_r = [n_e^2, n_o^2, n_o^2]$ [29], where φ is the rotation angle of the director of the NLC. It is worth noting that direction of the NLC director can be efficiently controlled using a static electric field. This is due to the good alignment of the NLC molecules according to the applied field. This can be experimentally achieved as described by Haakestad *et al.* [30] and Zografopoulos *et al.* [31]. The n_o and n_e of E7 material can be calculated using the following Cauchy models [29]:

$$n_{e,o} = A_{e,o} + \left(\frac{B_{e,o}}{\lambda^2}\right) + \left(\frac{C_{e,o}}{\lambda^4}\right) \tag{1}$$

where A_e, B_e, C_e, A_o, B_o, and C_o are the Cauchy coefficients that can be found at different temperatures in [32]. The Sellmeier equation of the soft glass of type SF57 is taken from [29]. However, the relative permittivity of the gold in the visible and near IR-region is expressed in [33].

The effective index of the NLC microstructured cladding at any wavelength is smaller than that of the soft glass background material. Therefore, the field is well confined in the core region due to the index contrast between the core and cladding regions. In this study, the effective indices of the core guided modes and surface plasmon modes are calculated using the full vectorial finite difference method (FVFDM) [24] with perfect matched layer boundary conditions. Additionally, the propagation through the axial direction of the proposed MUX/DEMUX is calculated by the CMT [5], [34]. The shortest length L_c, where the maximum power transfer from one core to the other core occurs, is defined as the coupling length and can be expressed as

$$L_c = \frac{\pi}{|\beta_e - \beta_o|} \tag{2}$$

where β_e, β_o are the propagation constants of the even and odd modes, respectively.

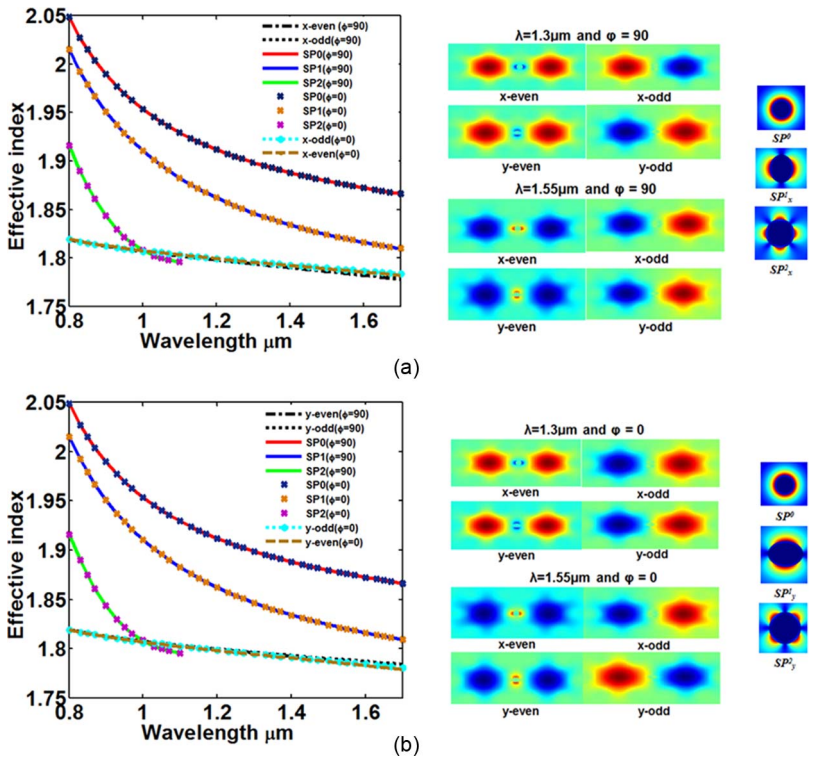

Fig. 2. Wavelength dependence of the effective indices of (a) x-polarized and (b) y-polarized core modes and surface Plasmon modes SP^0, SP^1_x, SP^1_y, SP^2_x, and SP^2_y.

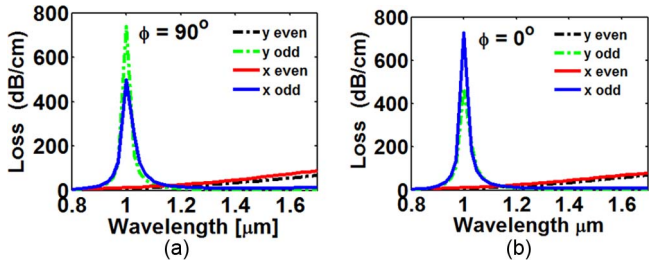

Fig. 3. Wavelength dependence on the losses of x- and y-polarization odd and even modes of the designed MUX/DEMUX at (a) $\varphi = 90^\circ$ and (b) $\varphi = 0^\circ$.

3. Numerical Results

The wavelength dependent effective indices and confinement losses of the even and odd modes of the x- and y-polarization states are shown in Figs. 2 and 3 at $\varphi = 0^\circ$ and 90°. Additionally, the effective indices of the surface plasmon modes, SP^o, SP^1_x, SP^1_y, SP^2_x and SP^2_y are also shown in Fig. 2. In this investigation, $d_C = 1.5\ \mu$m, $\Lambda = 2.725\ \mu$m, $d_m = 0.6\ \mu$m and the temperature is fixed to 25°C. The confinement loss is calculated from

$$loss = \frac{40\pi}{\ln(10)\lambda} \times \mathrm{Im}(n_{eff}) \times 10^4\ \mathrm{dB/cm} \tag{3}$$

where Im (n_{eff}) is the imaginary part of the complex effective index of the guided mode.

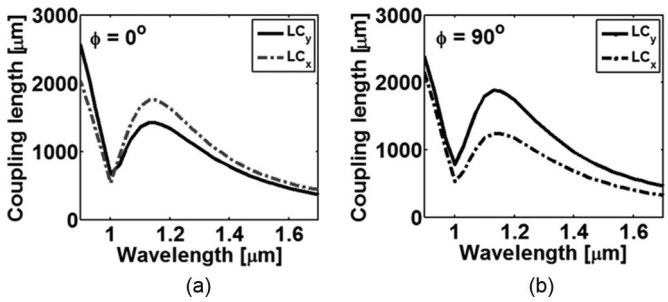

Fig. 4. Variation of the coupling length with the wavelength for x- and y-polarized modes of the reported MUX/DEMUX at (a) $\varphi = 90^\circ$ and (b) $\varphi = 0^\circ$.

Fig. 2 shows that the effective indices of the x and y-polarized dual core modes are smaller than that of most SP modes. In addition, the effective indices of the SP^2 and odd and even guided modes are phase matched at resonant wavelength λ_r of 1 μm. It is also revealed from Fig. 2 that the effective indices of the SP modes of the two polarized modes are independent on the rotation angle of the NLC. This is due to the well confinement of the SP modes around the central gold wire away from the NLC cladding structure, as shown in the field plot of Fig. 2(a) and (b). It is worth noting that the proposed design supports only one fundamental SP mode (SP^0). Therefore, the effective indices of the SP^0 shown in Fig. 2(a) and (b) are exactly the same. However, the differences between the effective indices of the x- and y-polarized SP modes, SP^1, and SP^2 are of order $(10^{-6} \sim 10^{-4})$ along the studied wavelength range. On the other hand, the differences between the effective indices of the x- and y-polarized states of the even and odd dual core modes are of order $(10^{-4} \sim 10^{-3})$. This is due to the overlap of the even and odd dual core modes with the infiltrated birefringent NLC cladding region, as shown in the field plot of Fig. 2.

To demonstrate the effect of the NLC infiltration, the proposed design with central gold wire but without NLC infiltration has been studied. The numerical results show that there is no effect of the NLC filling on the differences between the effective indices of the x- and y-polarized SP modes. This is due to the well confinement of the SP modes around the gold rod away from the NLC cladding microstructure. However, the differences between the effective indices of the x- and y-polarized states of the even and odd dual core modes are of lower order of $(10^{-5} \sim 10^{-4})$ than order of $(10^{-4} \sim 10^{-3})$ of the reported design with the NLC infiltration along the studied wavelength range. This means that the infiltration of the NLC increases the birefringence between x- and y- polarized dual core modes.

According to the attenuation loss behavior in Fig. 3, it is noted that the even and odd modes exhibit quite dissimilar losses at the resonant wavelength. As shown from this figure, the coupling between the odd modes of the two polarized modes at $\varphi = 0^\circ$ and 90° and SP^2 mode is strong at the resonance wavelength of 1 μm. At $\varphi = 90^\circ$, loss peaks of 498.63 and 738.79 dB/cm are achieved for the x- and y-polarized odd modes, respectively. However, at $\varphi = 0^\circ$, losses of 727.39 and 470.57 dB/cm are obtained at $\lambda_r = 1$ μm. However, the coupling between the two polarized even modes and the SP^2 is weak as shown in Fig. 3. It is also noted that there is no phase matching between the odd modes with the other SP modes in the wavelength region of interest, as shown in Fig. 2.

The variation of the coupling length of the designed MUX/DEMUX for x and y-polarized modes with the wavelength is displayed in Fig. 4 at $\varphi = 90^\circ$ and 0°. As the wavelength increases, the confinement of the modes through the core regions decreases. Therefore, the distance taken by the modes to transform from one core to the other core decreases. Consequently, the coupling length decreases with increasing the wavelength (normal behavior). This can be achieved through the studied wavelength range without using metallic rod. If the central gold rod is used, a strong phase matching between the surface plasmon modes and core guided modes occurs at

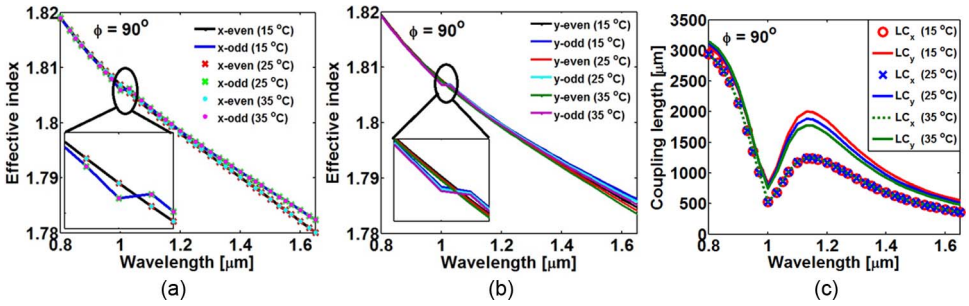

Fig. 5. Variation of the wavelength dependent effective indices of odd and even modes of (a) x-polarized and (b) y-polarized states. (c) The wavelength dependent coupling lengths of the two polarized states at different temperatures.

the resonance wavelength. At this point, the energy of the guided modes in x- and y-polarization states will couple to the surface plasmon modes around the central rod. As a result, the coupling length decreases suddenly to its minimum value at resonance wavelength $\lambda_r = 1$ μm, as is evident in Fig. 4. If the wavelength is further increased away from the resonance point, the coupling length should return to its normal behavior with the wavelength variation. Therefore, the coupling length first abruptly increases as an intermediate stage and then decreases by increasing the wavelength, as predicted.

The effect of the temperature variation on the coupling characteristics of the proposed design is also studied. In this investigation, the Cauchy coefficients of the NLC at different temperatures are taken from [32]. Fig. 5(a) and (b) show the wavelength dependent effective indices of the odd and even modes for x- and y-polarization states at $\varphi = 90^\circ$ at different temperatures 15 °C, 25 °C, and 35 °C. The corresponding coupling lengths for the two polarized modes are shown in Fig. 5(c). It is evident from these figures that the temperature has no effect on the effective indices and hence the coupling lengths of the x-polarized modes. At $\varphi = 90^\circ$, ε_r of the E7 material has the diagonal form $[n_o^2, n_e^2, n_o^2]$. Therefore, the x-polarized modes are dependent on n_o which has a slight variation with the temperature [32]. However, the y-polarized modes are mainly affected by n_e which is more temperature dependent than the n_o of the NLC of type E7. Therefore, the y-polarized modes are affected by the temperature change as shown in Fig. 5(b) and (c). As the temperature increases, the n_e and hence the cladding effective refractive index seen by the y-polarized modes decrease. Consequently, the effective indices of the y-polarized modes decrease by increasing the temperature from 15 °C to 35 °C as revealed from Fig. 5(b). The numerical results also show that the temperature variation has no effect on the effective indices and confinement losses of the surface plasmon modes. This is due to the well confinement of the surface plasmon modes around the gold wire away from the temperature dependent NLC infiltrated cladding region as shown in the field plot of Fig. 2. Furthermore, the temperature has no effect on the resonance wavelength of the odd modes at $\lambda_r = 1$ μm. It is worth noting that T. R. Wolinski *et al.* [35], [36] have experimentally demonstrated that the temperature can be controlled by using thermo-electric module that can control the temperature in the 10–120 °C range with 0.1 °C long-term stability and electric field regulation in the 0–1000 V range with frequencies from 50 Hz to 2 KHz.

The ratio between the coupling length at $\lambda = 1.3$ μm and 1.55 μm for x- and y-polarized modes at different lattice pitch values at $\varphi = 90^\circ$ and 0° is calculated from (4), shown below, and the results are shown in Fig. 6

$$\gamma_P = \frac{(L_{C1.3})_P}{(L_{C1.55})_P} \tag{4}$$

where P denotes x- or y-polarization state. Fig. 6 shows the variation between the γ ratio and the lattice constant for the two polarized modes at $\varphi = 90^\circ$ and 0°. As the hole pitch increases,

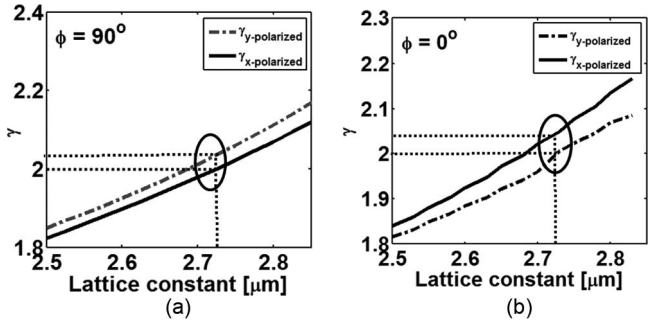

Fig. 6. Variation of the ratio between the coupling lengths at wavelengths of 1.3 μm and 1.55 μm for x-polarized and y-polarized modes with the hole pitch at (a) $\varphi = 90^\circ$ and (b) $\varphi = 0^\circ$.

TABLE 1

Coupling length (L_c) and the ratio γ of the suggested MUX/DEMUX at $\varphi = 90^\circ$ and 0° for the two polarized modes

		L_c of x-polarized state (μm)	L_c of y-polarized state (μm)	L_c of polarization-independent MUX/DEMUX $\frac{(L_{C1.3})_x + (L_{C1.3})_y}{2}$ (μm)
φ=90°	λ = 1.3μm	953.254	1322.86	1138.059
	λ = 1.55 μm	474.868	650.95	
	γ	2.0074	2.047	
φ=0°	λ = 1.3 μm	1251.69	1108.297	1179.99
	λ = 1.55 μm	615.081	552.031	
	γ	2.035	2.007	

the modes will be more confined in the high index solid core regions. Therefore, the modes will take longer distance to transfer from the first core to the other one. Consequently, the coupling length increases by increasing the hole pitch. In order to separate the two wavelengths 1.3 μm and 1.55 μm at the output of the designed MUX/DEMUX, the coupling length at $\lambda = 1.3$ μm should be a multiple integer of the coupling length at $\lambda = 1.55$ μm. To achieve the shortest device length, the value of γ_P should equal to 2. The results obtained from Figs. 4 and 6 are reported in Table 1. As can be seen from Table 1, the suggested structure can be used as a surface plasmon LC PCF MUX/DEMUX for x-polarized modes with device length as short as 953.254 μm and 1251.69 μm at φ equals to 90° and 0°, respectively. In addition, the same function is accomplished for the y-polarized modes with device length of 1322.86 μm and 1108.297 μm at $\varphi = 90^\circ$ and 0°, respectively. Moreover, the polarization independent can be achieved at device length equals to the average of coupling length of the x- and y-polarized modes at $\lambda = 1.3$ μm as shown in the last column of Table 1.

The normalized transmission powers of x- and y-polarized modes as a function of the propagation distance z in the core B of the designed MUX/DEMUX is calculated by the CMT and the obtained results are shown in Fig. 7 at $\varphi = 90^\circ$ and 0°. The normalized input power launched into core A is not completely transferred to the output core B due to the metal absorption loss. The crosstalk is a measure of the undesired power, or the power of the undesired wavelength, remaining at the output core. It is evident from Fig. 7 that the wavelengths of 1.3 μm and 1.55 μm can be separated at a device length of 953 μm and 1252 μm at $\varphi = 90^\circ$ and 0° for the x-polarized state, which is compatible with those reported in Table 1 calculated by the FVFDM. Additionally, y-polarized MUX/DEMUX can be achieved with device length of 1323 μm and 1108 μm at $\varphi = 90^\circ$ and 0°, respectively. Figs. 8 and 9 show the crosstalk around the operating wavelengths

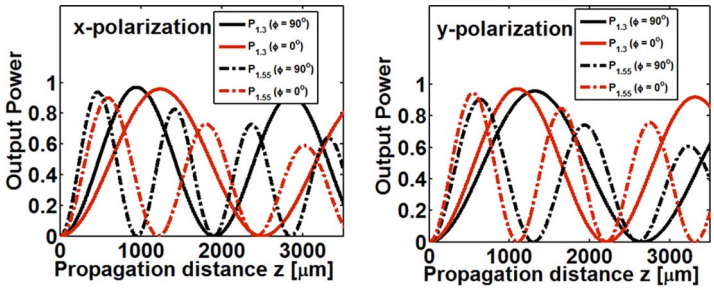

Fig. 7. Transmitted normalized power as a function of the propagation distance z at $T = 25\ ^{\circ}$C for (a) x-polarization and (b) y-polarization states.

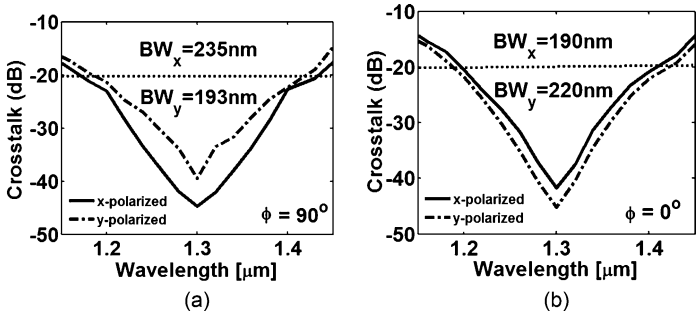

Fig. 8. Wavelength dependent crosstalk of the proposed MUX/DEMUX at core β around the operating wavelength $\lambda = 1.3\ \mu$m at (a) $\varphi = 90^{\circ}$ and (b) $\varphi = 0^{\circ}$.

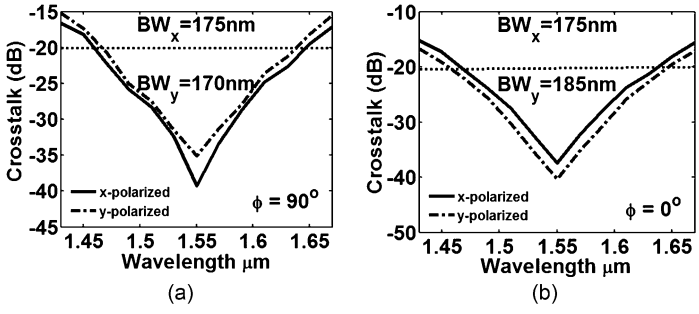

Fig. 9. Wavelength dependent crosstalk of the proposed MUX/DEMUX at core *B* around the operating wavelength $\lambda = 1.55\ \mu$m at (a) $\varphi = 90^{\circ}$ and (b) $\varphi = 0^{\circ}$.

for x- and y-polarized modes at $\varphi = 90^{\circ}$ and 0°, respectively. The crosstalk around wavelength of 1.3 μm at core *B* can be expressed as

$$CT_{1.3P} = 10\log_{10}\left(\frac{(P_{1.55})_{B.P}}{(P_{1.3})_{B.P}}\right)\ \text{dB} \tag{5}$$

where *P* is denoted for x- and y-polarization states. However, the crosstalk around $\lambda = 1.55\ \mu$m at core *A* is given by

$$CT_{1.55P} = 10\log_{10}\left(\frac{(P_{1.3})_{A.P}}{(P_{1.55})_{A.P}}\right)\ \text{dB}. \tag{6}$$

It is found that, at $\varphi = 90^{\circ}$, the proposed MUX/DEMUX has great bandwidths of 235 nm and 193 nm around $\lambda = 1.3\ \mu$m for x- and y-polarized modes, respectively. However, at $\varphi = 0^{\circ}$, the

bandwidth is as large as 190 nm and 220 nm for x- and y-polarized modes, respectively. In addition, bandwidths of 175 nm and 170 nm are obtained around $\lambda = 1.55$ μm for x- and y-polarized modes, respectively, at $\varphi = 90°$. Besides, at $\varphi = 0°$, the bandwidths of the proposed MUX/DEMUX are 175 nm and 185 nm around $\lambda = 1.55$ μm for x- and y-polarized modes, respectively. The bandwidths of the proposed MUX/DEMUX at the two different operating wavelengths are calculated with crosstalk better than –20 dB. If the device length is fixed to the 1138.059 μm and 1179.99 μm at $\varphi = 90°$ and 0°, respectively, the polarization independence multiplexing-demultiplexing is accomplished, as reported in Table 1.

It is worth noting from the crosstalk values that the proposed MUX/DEMUX has low sensitivity to the fabrication perturbation. The bandwidths of the suggested design are larger than those reported by Florous *et al.* [18], [21] with much shorter device lengths. In this regard, Florous *et al.* reported MUX-DEMUX of device length 15.4 mm [18] with bandwidths of 5.1 and 2.7 nm around wavelengths of 1.3 μm and 1.55 μm, respectively. Additionally, bandwidths of 5.5 and 2.0 nm have been reported with device length of 9.08 mm [21] around wavelengths of 1.3 μm and 1.55 μm, respectively. Further, the MUX-DEMUXs reported by Chen and Zhou [20] and Hameed *et al.* [29] have longer device length of 10.69 and 3.265 mm and smaller bandwidths than the reported design. Moreover, the suggested design has high tunability due to the infiltration of the NLC material.

The fabrication of the suggested MUX/DEMUX can be achieved by the widely used stack and draw technique [1]. During this process, the air holes can be arranged in a triangular lattice with high accuracy. Therefore, the position of the hollow channel that will be infiltrated by the gold can be controlled with high accuracy. The Ti:Sa laser assisted polymer gluing can then be utilized to selectively open or inflate the air holes with diameter down to 500 nm [37]. Then, the hollow channel can be filled by the gold at its melting point by using high pressure. Additionally, the infiltration of the cladding air holes by the NLC has been experimentally performed by using capillary forces as reported by Haakestad *et al.* [30]. Therefore, the fabrication of the suggested MUX/DEMUX can be fulfilled successfully.

4. Conclusion

A novel design of polarization independent surface plasmon MUX/DEMUX based on surface plasmon LC DC-PCF is reported and analyzed. Additionally, the effect of the structural geometrical parameters, rotation angle of the director of the NLC and temperature on the performance of the suggested MUX/DEMUX is studied. The infiltration of the NLC increases the birefringence between the two polarized beams. The numerical results show that the proposed design can separate the wavelengths of 1.55 μm and 1.3 μm with compact length and large bandwidths for the two polarized states. Additionally, polarization independent MUX/DEMUX can be obtained with device length of 1138.059 μm and 1179.99 μm at $\varphi = 90°$, and 0°, respectively.

References

[1] T. Birks, J. Knight, and P. Russell, "Endlessly single-mode photonic crystal fiber," *Opt. Lett.*, vol. 22, no. 13, pp. 961–963, 1997.
[2] M. F. O. Hameed, M. Abdelrazzak, and S. S. A. Obayya, "Novel design of ultra-compact triangular lattice silica photonic crystal polarization converter," *IEEE J. Lightw. Technol.*, vol. 31, no. 1, pp. 81–86, Jan. 2013.
[3] M. F. O. Hameed and S. S. A. Obayya, "Ultrashort silica liquid crystal photonic crystal fiber polarization rotator," *Opt. Lett.*, vol. 39, no. 4, pp. 1077–1080, 2014.
[4] M. F. O. Hameed and S. S. A. Obayya, "Coupling characteristics of dual liquid crystal core soft glass photonic crystal fiber," *IEEE J. Quantum Electron.*, vol. 47, no. 10, pp. 1283–1290, Oct. 2011.
[5] S. Zhang *et al.*, "Theoretical study of dual-core photonic crystal fibers with metal wire," *IEEE Photon. J.*, vol. 4, no. 4, pp. 1178–1187, Aug. 2012.
[6] Z. Fan *et al.*, "Numerical analysis of polarization filter characteristics of D-shaped photonic crystal fiber based on surface plasmon resonance," *Plasmonics*, vol. 10, no. 3, pp. 675–680, Jun. 2014.
[7] H. Tyagi *et al.*, "Plasmon resonances on gold nanowires directly drawn in a step-index fiber," *Opt. Lett.*, vol. 35, no. 15, pp. 2573–2575, 2010.
[8] W. Barnes, A. Dereux, and T. Ebbesen, "Surface plasmon subwavelength optics," *Nature*, vol. 424, pp. 824–830, Aug. 2003.

[9] Z. Tan *et al.*, "Phase modulation and structural effects in a D-shaped all-solid photonic crystal fiber surface plasmon resonance sensor," *Opt. Exp.*, vol. 22, no. 12, pp. 15049–15063, 2014.
[10] M. F. O. Hameed, A. M. Heikal, B. M. Younis, M. Abdelrazzak, and S. S. A. Obayya, "Ultra-high tunable liquid crystal-plasmonic photonic crystal fiber polarization filter," *Opt. Exp.*, vol. 23, no. 6, pp. 7007–7020, 2015.
[11] X. Shan, U. Patel, S. Wang, R. Iglesias, and N. Tao, "Imaging local electrochemical current via surface plasmon resonance," *Science*, vol. 327, no. 5971, pp. 1363–1366, Mar. 2010.
[12] G. Steiner, "Surface plasmon resonance imaging," *Anal. Bioanal. Chem.*, vol. 379, no. 3, pp. 328–331, 2004.
[13] P. Geng *et al.*, "Orthogonal single-polarization single-core photonic crystal fiber for wavelength splitting," *IEEE Photon. Technol. Lett.*, vol. 24, no. 15, pp. 1304–1306, Aug. 2012.
[14] L. Rosa, F. Poli, M. Foroni, A. Cucinotta, and S. Selleri, "Polarization splitter based on a square-lattice photonic-crystal fiber," *Opt. Lett.*, vol. 31, no. 4, pp. 441–443, 2006.
[15] S. Yang *et al.*, "Experimental study of mode field evolution of dual-core photonic crystal fiber," *IEEE Photon. Technol. Lett.*, vol. 19, no. 19, pp. 1523–1525, Oct. 2007.
[16] M. F. O. Hameed, K. Al Begain, A. M. Nasr, M. Abo el Maaty, and S. S. A. Obayya, "Coupling characteristics of a soft glass nematic liquid crystal photonic crystal fibre coupler," *IET Optoelectron.*, vol. 3, no. 6, pp. 264–273, Dec. 2009.
[17] K. Saitoh, Y. Sato, and M. Koshiba, "Coupling characteristics of dual-core photonic crystal fiber couplers," *Opt. Exp.*, vol. 11, no. 24, pp. 3188–3195, 2003.
[18] N. Florous, K. Saitoh, and M. Koshiba, "A novel approach for designing photonic crystal fiber splitters with polarization-independent propagation characteristics," *Opt. Exp.*, vol. 13, no. 19, pp. 7365–7373, 2005.
[19] L. Zhang and C. Yang, "Polarization-dependent coupling in twin-core photonic crystal fibers," *J. Lightw. Technol.*, vol. 22, no. 5, pp. 1367–1373, May 2004.
[20] M. Chen and J. Zhou, "Polarization-independent splitter based on all-solid silica-based photonic crystal fibers," *J. Lightw. Technol.*, vol. 24, no. 12, pp. 5082–5086, Dec. 2006.
[21] N. Florous, K. Saitoh, and M. Koshiba, "Synthesis of polarization-independent splitters based on highly birefringent dual-core photonic crystal fiber platforms," *IEEE Photon. Technol. Lett.*, vol. 18, no. 11, pp. 1231–1233, Jun. 2006.
[22] K. Chiang *et al.*, "Experimental demonstration of intermodal dispersion in a two-core optical fibre," *Opt. Commun.*, vol. 143, no. 4–6, pp. 189–192, Nov. 1997.
[23] Q. Li, Y. Song, G. Zhou, Y. Su, and M. Qiu, "Asymmetric plasmonic-dielectric coupler with short coupling length, high extinction ratio, and low insertion loss," *Opt. Lett.*, vol. 35, no. 19, pp. 3153–3155, 2010.
[24] A. Fallahkhair, K. Li, and T. Murphy, "Vector finite difference mode solver for anisotropic dielectric waveguides," *J. Lightw. Technol.*, vol. 26, no. 11, pp. 1423–1431, Jun. 2008.
[25] W. Huang, "Coupled-mode theory for optical waveguides: An overview," *J. Opt. Soc. Amer. A*, vol. 11, no. 3, pp. 963–983, 1994.
[26] K. Okamoto, *Fundamentals of Optical Waveguides*, 2nd ed. New York, NY, USA: Academic, 2005.
[27] J. Hou *et al.*, "Metallic mode confinement in microstructured fibres," *Opt. Exp.*, vol. 16, no. 9, pp. 5983–5990, 2008.
[28] A. Nagasaki, K. Saitoh, and M. Koshiba, "Polarization characteristics of photonic crystal fibers selectively filled with metal wires into cladding air holes," *Opt. Exp.*, vol. 19, no. 4, pp. 3799–3808, 2011.
[29] M. F. O. Hameed, S. S. A. Obayya, and R. Wiltshire, "Multiplexer demultiplexer based on nematic liquid crystal photonic crystal fiber coupler," *Opt. Quantum Electron.*, vol. 41, no. 4, pp. 315–326, Mar. 2009.
[30] M. W. Haakestad *et al.*, "Electrically tunable photonic bandgap guidance in a liquid-crystal-filled photonic crystal fiber," *IEEE Photon. Technol. Lett.*, vol. 17, no. 4, pp. 819–821, Apr. 2005.
[31] D. C. Zografopoulos, E. E. Kriezis, and T. D. Tsiboukis, "Photonic crystal-liquid crystal fibers for single-polarization or high-birefringence guidance," *Opt. Exp.*, vol. 14, no. 2, pp. 914–925, 2006.
[32] J. Li, S. Wu, S. Brugioni, R. Meucci, and S. Faetti, "Infrared refractive indices of liquid crystals," *J. Appl. Phys.*, vol. 97, no. 7, 2005, Art. ID. 073501.
[33] A. M. Heikal, M. F. O. Hameed, and S. S. A. Obayya, "Improved trenched channel plasmonic waveguide," *J. Lightw. Technol.*, vol. 31, no. 13, pp. 2184–2191, Jul. 2013.
[34] T. Feng, G. Feng, Y. Wu, and P. Ye, "Improved coupled-mode theory of anisotropic optical waveguides," *IEEE J. Quantum Electron.*, vol. 25, no. 3, pp. 249–251, Mar. 1989.
[35] T. R. Wolinski *et al.*, "Polarization effects in photonic liquid crystal fibers," *Meas. Sci. Technol.*, vol. 18, pp. 3061–3069, 2007.
[36] T. R. Wolinski *et al.*, "Influence of temperature and electrical fields on propagation properties of photonic liquid-crystal fibres," *Meas. Sci. Technol.*, vol. 17, no. 5, pp. 985–991, 2006.
[37] H. Lee, "Plasmonic photonic crystal fiber," Ph.D. dissertation, Max Plank Inst., Munich, Germany, 2012.